Characterization of high harmonic frequencies in reactor noise experiments within the CORTEX project

Klemen Ambrožič, Vincent Lamirand and Andreas Pautz

***Abstract*—We present a novel technique of neutron noise detection and experimental data interpretation developed during the EU H2020 project CORTEX aiming to improve the capabilities for identification and localization of neutron noise sources.**
The experimental data analysis is performed in the frequency domain by extracting the spectral power density and the phase angle using a novel spectral variance reduction technique based on per cycle based bootstrapping with replacement. This technique allows for variance reduction of measured spectral power and phase angle not only at base frequency but at higher harmonic frequency contributions as well. This allows for a more representative treatment of experimental data and validation of codes for neutron noise propagation, some of which have been developed within the project.
The detector response is not necessarily linearly dependent on the oscillator movement, and the study of non-linear terms provides additional information which can improve the accuracy of neutron noise source identification and localization. Moreover those terms can be used in a Taylor series to identify a more complex dependence. The process is simplified in the sense, that these contributions are linearized in the frequency domain as higher harmonic frequency contributions and can be easily identified and extracted due to spectral peaks prominence provided by the bootstrapping with replacement method. Combined with the spectral power and phase, we present a preliminary investigation of usability of higher order terms for noise source identification and localization.
In this paper, we outline the CORTEX project, the experiments and the measurement analysis methodology based on the bootstrapping with replacement along with the initial developments on the study of non-linear terms in CROCUS reactor, using several different noise source configurations at a set frequency.

***Index Terms*—bootstrapping, neutron detection, neutron noise, non-linear effects**

I. Introduction

THE neutron noise is the term used for neutron flux fluctuations about its mean value, and carries information about the processes occurring inside a nuclear reactor due to mechanical vibration, turbulence or boiling [1], [2]. It provides useful information on reactor operation and possible deviations, which might be indicative of abnormal operation or malfunction and may need to be addressed immediately [3]–[5]. The capability to identify and localize it's source is therefore of great significance.

The aim of the EU H2020 CORTEX project [6] is to develop tools and techniques for the localization and identification of noise sources by neutron flux measurements using multiple detectors. This is performed by analyzing the measured data by machine learning algorithms [7], [8], which have been previously trained using validated neutron noise propagation simulation computer codes [9]–[15]. The code validation is also performed within the scope of this project by performing experiments at zero power reactor facilities capable of inducing neutron noise: the Techniche Universität Dresden (TUD) Ausbildungskernreactor 2 (AKR-2) [16] equipped with a rotating and oscillating neutron absorber, entering the core from the side through its experimental channels (Figure 1) and the École Polytechnique Fédérale de Lausanne (EPFL) CROCUS reactor [17] with CROCUS Oscillator for Lateral Increase Between U-metal Rods and Inner zone (COLIBRI) experiment [18] located inside the reactor pool on the west side, oscillating up to 18 fuel rods and Pile Oscillator for Localized and Low Effect Noise (POLLEN) oscillating neutron absorber [19] usually installed at the core center. Both are displayed in Figure 2. In both cases, the oscillator pairs can perform synchronous operation. During experimental campaigns, both reactors were equipped with a variety of neutron detectors, ranging from ^3He, BF_3, fission and compensated boron chambers and optical fiber based detectors [20], some operating pulse mode whereas the others in current mode. An array of high-performance data acquisition systems with sufficient acquisition rate is used for data collection [21]–[23].

In order to perform the validation, the quantities of interest (QOI) to compare between computer codes and experiments have been established. The analysis is performed in the frequency domain, where spectral power and phase angle are calculated from measured detector response. In order to avoid difficulties associated with the absolute measurements, it was decided that spectral power ratio and phase angle difference with respect to the oscillator movement or a reference detector are used as QOI. The process is described in more detail in Section II. A single evaluation of QOI gives a relative variance of 1, since the length of the data set contributes only towards an increase in frequency resolution [24]. Variance reduction techniques such as Welch's method [5], [25] are usually used,

Submitted to IEEE Transactions on nuclear science on March 15, 2022. The research leading to these results has received funding from the Euratom research and training programme 2014-2018 under grant agreement No 754316.

Klemen Ambrožič is a postdoctoral researcher at Laboratory for Reactor Physics and Systems Behaviour at École Polytechnique Fédérale de Lausanne, Switzerland e-mail: klemen.ambrozic@epfl.ch

Vincent Lamirand is the head of experimental activities at Laboratory for Reactor Physics and Systems Behaviour at École Polytechnique Fédérale de Lausanne, Switzerland e-mail: vincent.lamirand@epfl.ch

Andreas Pautz is the head of the Laboratory for Reactor Physics and Systems Behaviour at École Polytechnique Fédérale de Lausanne, Switzerland e-mail: andreas.pautz@epfl.ch

(a) Rotating neutron absorber device.

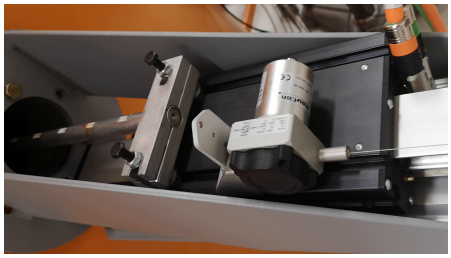

(b) Vibrating neutron absorber device .

Fig. 1: Rotating and vibrating neutron absorber devices mounted at the entrance of TUD AKR2 horizontal experimental channels.

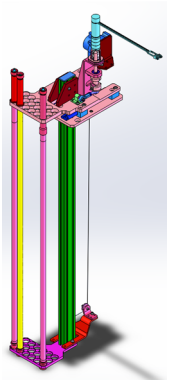

(a) COLIBRI fuel oscillating device CAD drawing.

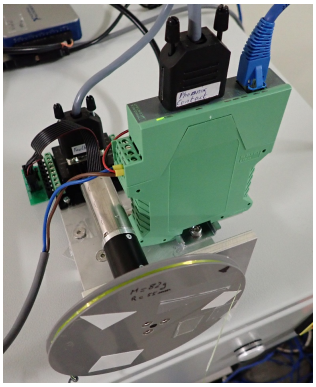

(b) The stepper motor, driving the Cd absorber of the POLLEN oscillator.

Fig. 2: COLIBRI fuel rod oscillator and POLLEN pile oscillator at the EPFL CROCUS reactor.

which have some shortcomings, most notably the phase angle uncertainty dependence on the section size.

A new method for variance reduction based on the per oscillation cycle bootstrapping is developed, which suppresses the signal outside the base and higher harmonic frequencies, decouples the correlations between consecutive cycles, does not reduce the underlying frequency resolution and allows for an unambiguous determination of spectral power, phase angle and their ratios/differences. The analysis method has been applied to experiments performed at both CROCUS and AKR-2 reactors, showing good agreement with calculated results [26].

As mentioned, the analysis technique based on the bootstrapping with replacement suppresses all the frequencies outside the base and higher harmonic frequencies and their spreads, which means several spectral peaks can be easily identified. Moreover, during the second experimental campaign at the CROCUS reactor, the COLIBRI oscillator was operated at a set frequency and 4 configurations of oscillating fuel. The data from these experiments was used for the preliminary analysis of non-linear terms, to investigate if this information can be used to further improve on the noise source localization and identification.

The paper starts by describing the general analysis methodology and extraction of spectral power ratio and phase angle difference and continues with the focus on derivation of non-linear contributions and its preliminary application to the above mentioned measurements at CROCUS reactor. Some conclusions will be drawn at the end with a short discussion on future developments.

II. Analysis Methodology

In this section, the basics of the analysis method are explained as a more detailed description and study of the analysis methodology is provided in [27].

The analysis is performed in the frequency domain. However, in order to decouple the measured data from the reactor power, effecting the amplitude of induced neutron noise, the data standardization must be performed first by dividing and subtracting a moving average i.e. the reactor power mean. One must keep in mind that this procedure changes the frequency response compared to the original signal, and entire data set should be processed the same way in order to be consistent. The standardized signal is then transformed into frequency domain using the Fourier transform, as displayed in Equation 1.

$$X_i(f) = FFT(x_i(t)) \tag{1}$$

where $x_i(t)$ denotes the standardized time series of detector signal or oscillator position, and $X_i(f)$ is the Fourier transform respectively. By having multiple time series, one can construct a cross correlation function $h_{i,j}(f)$ in Equation 2

$$h_{i,j}(f) = X_i(f) \cdot X_j(f)^* \tag{2}$$

where * denotes the complex-conjugate. This function is used to calculate the spectral power density estimate ($PSD_{i,j}(f)$) and spectral power $PS_{i,j}(f_k)$ as well as the phase angle $\phi_{i,j}(f_k)$ between the two signals i and j. Another useful measure of linear correlation is coherence $COH_{i,j}$. The derivation of these expressions is displayed in Equation 3.

$$\begin{aligned} PS_{i,j}(f_k) &= \int_{f_k} PSD_{i,j}(f)df \approx \int_{f_k} |h_{i,j}(f)|^2 df \\ \phi_{i,j}(f_k) &\approx arg(h_{i,j}(f_k)) \\ COH_{i,j}(f_k) &= \frac{|h_{i,j}(f_k)|^2}{h_{i,i}(f_k)h_{j,j}(f_k)} \end{aligned} \tag{3}$$

The actual QOI are spectral power ratios and phase angle differences with respect to the oscillator or a reference detector as displayed in Equation 4. In case of code validation, the selected reference detector was usually the one furthest away from the oscillation source, exhibiting most point kinetic behaviour.

$$\begin{aligned} \widetilde{PS}_{i,ref}(f_k) &= \frac{PS_{i,j}(f_k)}{PS_{j,ref}(f_k)} = \sqrt{\frac{PS_{i,i}(f_k)}{PS_{ref,ref}(f_k}}) \\ \widetilde{\phi}_{i,ref}(f_k) &= \phi_{i,j}(f_k) - \phi_{j,ref}(f_k) \end{aligned} \tag{4}$$

The approximation sign in Equation 3 is related to the above mentioned variance. Welch's approach remedies this, by sectioning the time series into equal blocks on which Fourier transform is performed, with the final result being QOI mean and standard deviation as maximum likelihood and confidence interval respectively, which is not the case [28], [29], especially with correlations. However, one must note

that this process reduces the frequency resolution, propagates correlations in time by drawing a series of consecutive oscillation responses and has a phase angle uncertainty dependence on the block size. The issue is exacerbated by having a variation of cycle lengths due to mechanical play in the neutron noise inducing oscillator.

To remedy these shortcomings, a method based on bootstrapping with replacement [30], [31] with blocks corresponding to oscillator cycles has been developed. The method works by sectioning the original data series by oscillation cycles as precisely as possible, and reconstructing a proxy time series (Figure 3), from which the desired QOI are calculated. The sectioning by cycles is crucial, as the proxy signal coherence is lost otherwise, increasing the noise.

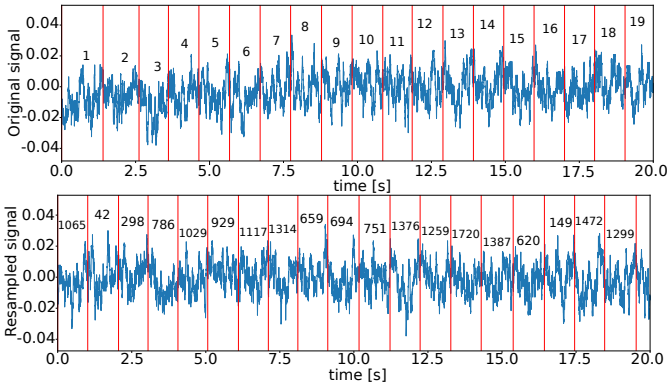

Fig. 3: Example of original (top) and the re-sampled (bottom) time series with numbers on top indicating the consecutive oscillation number in the original sample.

The re-sampling process is repeated a great number of times in order to obtain a statistically significant sample, which can be processed under the assumption of normal distribution as an estimate, or by storing the QOI of each individual re-sampling and constructing a histogram, from which the QOI maximum likelihood and confidence interval can be obtained. The re-sampling does not reduce the frequency resolution and it decouples the correlations between individual oscillator cycles. The phase angles are always resolved, even at oscillation cycle length deviations of few percent. An additional advantage of per-cycle based bootstrapping with re-sampling is its frequency response function, passing through only the base frequency and higher harmonic components, suppressing the rest, as displayed in Figure 4. On the other hand, the process is much more computationally expensive due to calculation of a large number of Fourier transforms. While most of the code was written in Python [32], [33] using optimized numerical libraries [34], [35], the code was accelerated by porting the Fourier transform to a graphics processor [36] and construction of proxy signals using a custom Fortran [37] code. Storing the QOI over the entire frequency range for each re-sampling is still prohibitively expensive in terms of computer storage. Therefore the processing is performed in three steps:

1) Initial bootstrapping is performed over a large frequency range, usually up to 10 times the base frequency, using simple mean.

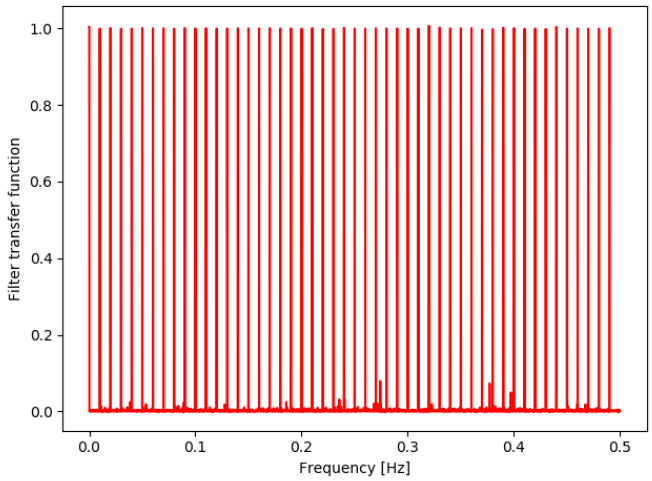

Fig. 4: Frequency response function of the bootstrapping process with oscillator cycle frequency of 0.01 Hz.

2) Spectral power peaks and integration ranges are identified.
3) QOI of during individual cycle are calculated and stored for histogram construction, from which maximum likelihood and confidence interval are determined.

This allows for evaluation of QOI, their best estimate and uncertainty (BEPU) to be unbiased and without assumptions on distributions and correlations, exploring the entirety of the phase space obtained from measurements. A comparison between spectral power evaluated using the cycle-based bootstrapping with replacement and the Welch's approach can be observed in Figure 5, with higher harmonic frequencies spectral peaks are clearly resolved using the bootstrapping technique. The exact resolution of QOI and the presence of spectral peaks at higher harmonic frequencies allows for the study of higher harmonic frequencies, which may result from a situation displayed in Figure 6, inducing non-linear components at higher harmonic frequencies. The evaluations of coherence between oscillator movement and the detector signal also never quite reaches 1 which suggests the presence of non-linear terms. This kind of analysis could improve the identification and localization of the noise source.

III. Non-linear effects

The oscillators movement effects on the detector signal are by no means limited to linear terms. In case of a fuel rod or neutron absorber oscillating in-between several fuel rods might be in favour of quadratic or even higher order response due to the effects of its position on moderation, absorption and fission. The oscillator movement itself can generally comprise of several frequency components at base and higher harmonic frequencies, either intentionally or due to its construction. The oscillator movement in time can be described by Equation 5.

$$Osc(t) = \sum_k B_k \cdot sin(k\omega_0 t + \delta_k) \tag{5}$$

where $Osc(t)$ is the detector movement in time, B_k the amplitude and δ_k the phase shift of order k. As mentioned,

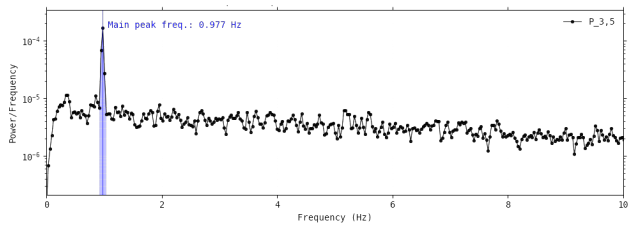

(a) Welch's approach.

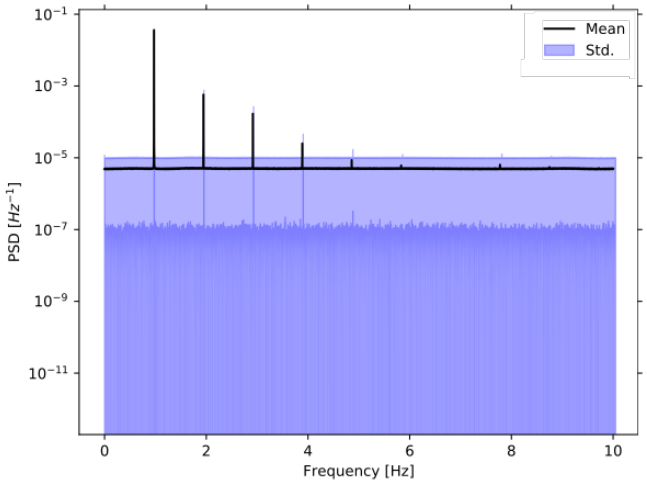

(b) Bootstrapping approach.

Fig. 5: Comparison of Welch's and bootstrapping with replacement spectral power variance reduction technique.

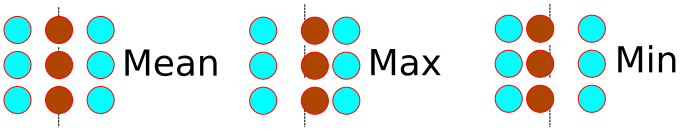

Fig. 6: A schematic of oscillating fuel rods inside a typical PWR fuel element, where the quadratic term of oscillator movement contributes mostly to the reactor noise.

the detector response can also be written as a power series of the oscillator movement, as displayed in Equation 6.

$$D(t) = \sum_j A_j \cdot Osc(t)^j \tag{6}$$

where $D(t)$ is the detector response in time and A_j the amplitude of order j. These higher order contributions can

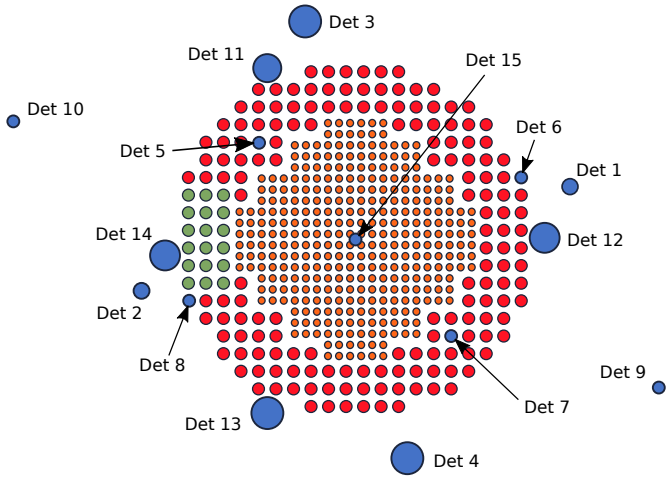

Fig. 7: Detector layout during 2nd experimental campaign at CROCUS reaactor. Green circles denote the fuel elements, which can be oscillated by the COLIBRI experiment.

be easily expanded as displayed in Equation 7.

$$\begin{aligned}
Osc^2(t) &= \sum_k \frac{1}{2} B_k^2 \left[1 + sin\left(2k\omega_0 t + 2\delta_k - \frac{\pi}{2}\right)\right] \\
Osc^3(t) &= \sum_k \frac{1}{4} B_k^3 \big[3sin\left(k\omega_0 t + \delta_k\right) + \\
&\qquad sin\left(3k\omega_0 t + 3\delta_k - \pi\right)\big] \\
Osc^4(t) &= \sum_k \frac{1}{8} B_k^4 \big[3 + 4sin\left(2k\omega_0 t + 2\delta_k\right) + \\
&\qquad sin\left(4k\omega_0 t + 4\delta_k + \frac{\pi}{2}\right)\big] \\
Osc^5(t) &= \sum_k \frac{1}{16} B_k^5 \big[10sin\left(k\omega_0 t + \delta_k\right) + \\
&\qquad 5sin\left(3k\omega_0 t + 3\delta_k - \pi\right) + \\
&\qquad sin\left(5k\omega_0 t + 5\delta_k\right)\big] \\
&\vdots
\end{aligned} \tag{7}$$

By inserting Equation 7 into Equation 6, one can determine A_i terms in two ways: comparing either amplitudes i.e. square root of spectral power or by comparing phase angles. In the present paper, comparison using spectral power is performed on a select few measurements of the second experimental campaign at CROCUS reactor, where the COLIBRI fuel rod oscillator loading was different for each measurement.

The 2nd experimental campaign at the CROCUS reactor was performed in November, 2019 with 15 neutron detectors installed as depicted in Figure 7. Further details can be found in the report [38]. In total 31 experiments were performed with 4 distinct loading patterns of the COLIBRI oscillator, oscillation amplitude of 1.5 mm and oscillation frequencies 0.1 and 0.97 Hz respectively. For the analysis of higher order contributions, 5 different COLIBRI loading patterns were used, as displayed in Table I. The COLIBRI position numbering convention is schematically displayed in Figure 8.

The above mentioned bootstrapping with replacement method was used with simple mean as maximum likelihood

TABLE I: Measurements of the 2nd experimental campaign at CROCUS reactor used in the analysis.

Experiment number	Oscillated rods	Amplitude [mm]	Frequency [Hz]
18	A1-C3	1.5	0.97
24	A4-C6	1.5	0.97
27	C1	1.5	0.97
31	C6	1.5	0.97

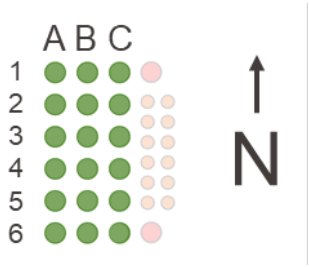

Fig. 8: COLIBRI fuel rod position naming convention. Reactor core fuel elements denoted in red.

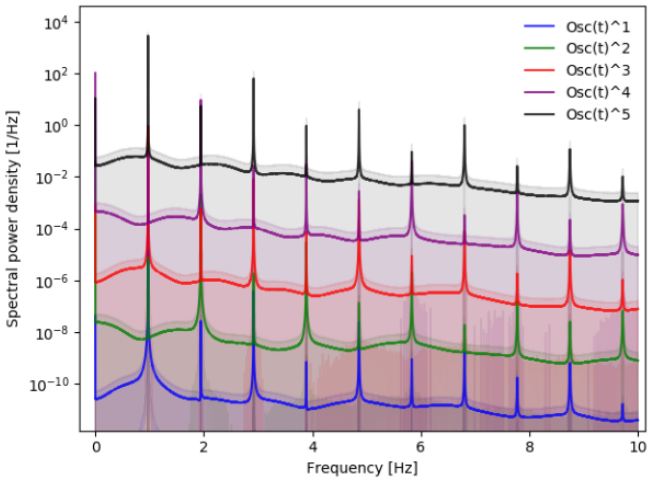

Fig. 9: Auto spectral power densities of the oscillator movement and its higher orders.

value and standard deviation as the confidence interval to calculate the spectral power density of detector responses the COLIBRI oscillator and its higher orders, displayed in Figure 9 for measurement no. 27. Up to 5th order effects are considered. We are not interested in the cross-spectral terms, hence only terms $i = j$ from Equation 2 are used. The spectral power peak locations and their integration extents were calculated according to [27] to calculate the spectral power and amplitudes B_i from Equation 5 respectively. The comparison is valid even after the signal standardization due to same moving average window being used for all the data sets and its effects on the calculations of spectral power density are the same. These results are then used to construct the series in Equation 6 by adjusting A_j terms using the least squares method. This analysis has been performed for all of the detectors, in order to observe a general behaviour or identify potential detector outliers, where the effect of higher orders differs from the rest. Results from these analysis for the above mentioned COLIBRI loading patterns are displayed in Figures 10 to 13, where a difference between individual experiments can be observed. Loading the northern side of COLIBRI seems to induce less higher order effects compared to loading the southern side. Moreover, the effect seems to be most prominent, when comparing loading at C1 and C6 positions. Contributions to various detector signals also show some deviation, for example det. 11 and 13 of measurement no. 18 shows higher degree of A_i term oscillation. Although these detectors are located symmetrically with respect to the whole COLIBRI, the A_i terms seem to be significantly alternating in magnitude. On the other hand, no such effect is visible, when comparing detectors 3 and 4, which are also positioned symmetrically. This would indicate some sort of spatial distribution of propagated higher orders, and will have to be studied in the future experiments.

Although the analysis is performed considering a simple mean and standard deviation as maximum likelihood and confidence interval values, we can observe that minor changes in the number and position of the oscillating fuel rods significantly change the detector response in terms of higher modes. This is indeed very encouraging for future developments as additional information for localization and identification of reactor noise sources.

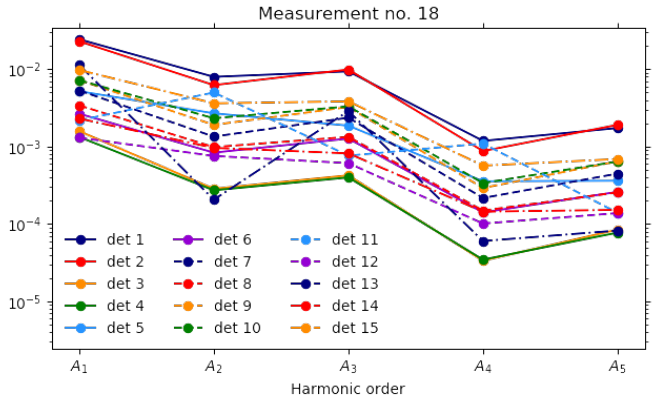

Fig. 10: A_i terms of measurement no. 18, COLIBRI loading: A1-C3.

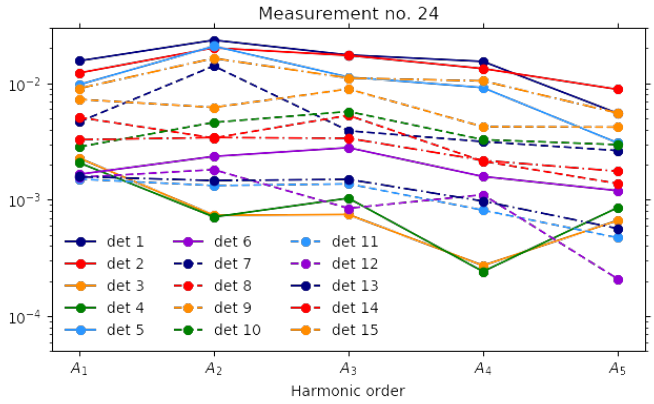

Fig. 11: A_i terms of measurement no. 24, COLIBRI loading: A4-C6.

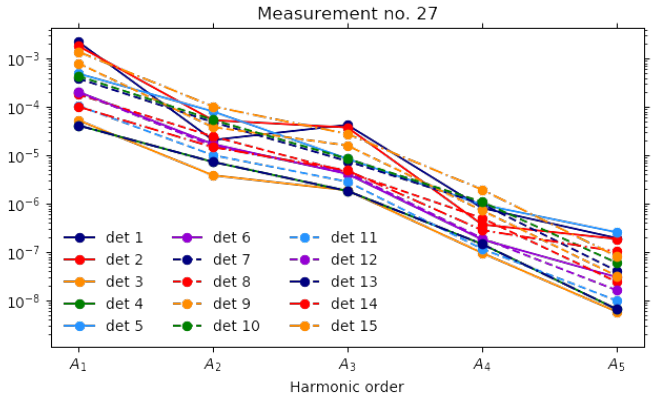

Fig. 12: A_i terms of measurement no. 27, COLIBRI loading: C1.

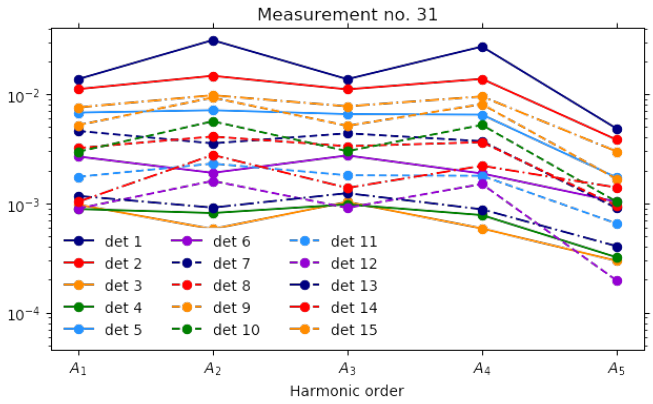

Fig. 13: A_i terms of measurement no. 31, COLIBRI loading: C6.

IV. Conclusions

The analysis of the oscillator movement and neutron detector time series based on the per-cycle bootstrapping with replacement technique allows for precisely distinguishing of the spectral peaks. The experimental data analyzed with this method provided data on spectral power and phase angle values, which have served for validation of neutron noise simulation codes developed or improved within the H2020 CORTEX project.

Suppression of spectral noise and increased prominence of spectral peaks at base and higher harmonic frequencies has enabled us to perform the investigation on non-linear term. Measurements of the 2nd experimental campaign at the CROCUS reactor were analyzed, where the COLIBRI fuel rod oscillator is loaded with 4 distinct configurations. Significant differences in propagation of higher oscillator contributions can be observed with respect to the number and position of the oscillating fuel rods.

V. Future outlooks

Investigation into non-linear terms presented in this paper deals only with the simple mean and standard ddeviation of spectral power. For future analysis, per re-sampling QOI results will be tracked for histogram construction and determination of maximum likelihood and confidence intervals. This analysis also does not take into account the phase angle. It would be interesting to observe if multiple peaks exist in the phase angle distribution, provided a sufficiently large number of QOI calculations from re-sampled data is obtained or by introducing a biased sampling procedure for the bootstrapping process.

Experiments with up to 150 miniature fiber based neutron detectors located in-between fuel elements are currently being prepared. This will allow for a detailed mapping of neutron flux, neutron noise propagation and the propagation of higher orders of neutron noise, which would be unprecedented. In terms of computational requirements, the analysis of such large data sets would be a huge task, hence the code is currently being rewritten to allow for inter-node communication with MPI [39], [40] and multiple GPU nodes using technologies like NVCC [41] for utilization of large computer clusters.

VI. Copyright notice

References

[1] U. Rohde, M. Seidl, S. Kliem, and Y. Bilodid, "Neutron noise observations in german kwu built pwrs and analyses with the reactor dynamics code dyn3d," *Annals of Nuclear Energy*, vol. 112, pp. 715–734, 2018.

[2] L. Torres, D. Chionis, C. Montalvo, A. Dokhane, and A. García-Berrocal, "Neutron noise analysis of simulated mechanical and thermal-hydraulic perturbations in a pwr core," *Annals of Nuclear Energy*, vol. 126, pp. 242–252, 2019.

[3] J. A. Thie, "Elementary methods of reactor noise analysis," *Nuclear Science and Engineering*, vol. 15, no. 2, pp. 109–114, 1963.

[4] V. Verma, D. Chionis, A. Dokhane, and H. Ferroukhi, "Studies of reactor noise response to vibrations of reactor internals and thermal-hydraulic fluctuations in pwrs," *Annals of Nuclear Energy*, vol. 157, p. 108212, 2021.

[5] J. A. Thie, *Power reactor noise*. American Nuclear Society.

[6] C. Demaziére, P. Vinai, M. Hursin, S. Kollias, and J. Herb, "Overview of the cortex project," in *Reactor Physics paving the way towards more efficient systems (PHYSOR 2018), Cancun, Mexico, 22-26 April, 2018*, Zenodo, Apr. 2018.

[7] Ioannou, George, Tagaris, Thanos, Alexandridis, Georgios, and Stafylopatis, Andreas, "Intelligent techniques for anomaly detection in nuclear reactors," *EPJ Web Conf.*, vol. 247, p. 21011, 2021.

[8] C. Demazière, A. Mylonakis, P. Vinai, A. Durrant, F. De Sousa Ribeiro, J. Wingate, G. Leontidis, and S. Kollias, "Neutron noise-based anomaly classification and localization using machine learning," *EPJ Web Conf.*, vol. 247, p. 21004, 2021.

[9] T. Yamamoto, "Implementation of a frequency-domain neutron noise analysis method in a production-level continuous energy monte carlo code: Verification and application in a bwr," *Annals of Nuclear Energy*, vol. 115, pp. 494–501, 2018.

[10] A. Mylonakis, P. Vinai, and C. Demazière, "Core sim+: A flexible diffusion-based solver for neutron noise simulations," *Annals of Nuclear Energy*, vol. 155, p. 108149, 2021.

[11] Verma, V., Chionis, D., Dokhane, A., and Ferroukhi, H., "Modelling and analysis of fuel assembly vibrational modes in pwrs using simulate-3k," *EPJ Web Conf.*, vol. 247, p. 21008, 2021.

[12] I. Pázsit and C. Demaziere, "Noise techniques in nuclear systems," in *Handbook of Nuclear Engineering*, 2010.

[13] Rouchon, Amélie, Le Brun, Malkiel Vadée, and Zoia, Andrea, "Analysis and comparison of apollo3 and tripoli-4 neutron noise solvers," *EPJ Web Conf.*, vol. 247, p. 21002, 2021.

[14] A. Gammicchia, S. Santandrea, I. Zmijarevic, R. Sanchez, Z. Stankovski, S. Dulla, and P. Mosca, "A moc-based neutron kinetics model for noise analysis," *Annals of Nuclear Energy*, vol. 137, p. 107070, 2020.
[15] H. Yi, P. Vinai, and C. Demazière, "Acceleration of a 2-dimensional, 2-energy group neutron noise solver based on a discrete ordinates method in the frequency domain," *EPJ Web Conf.*, vol. 247, p. 21005, 2021.
[16] Techniche Universität Dresden, Faculty of Mechanical Science and Engineering Institute of Power Engineering, "Training Reactor AKR-2-Description of the Reactor Facility Procedure of Operation," 2019. Accessed: 2021-08-19.
[17] U. Kasemeyer, R. Früh, J. Paratte, and R. Chawla, "Benchmark on Kinetic Parameters in the CROCUS Reactor," 2007.
[18] V. Lamirand, P. Frajtag, D. Godat, O. Pakari, A. Laureau, A. Rais, M. Hursin, G. Hursin, C. Fiorina, and A. Pautz, "The colibri experimental program in the crocus reactor: characterization of the fuel rods oscillator," *EPJ Web Conf.*, vol. 225, p. 04020, 2020.
[19] A. Rais, *Performance assessment of a 3-D steady-state and spatial kinetics model for the CROCUS reactor*. PhD thesis, Lausanne, 2018.
[20] V. Lamirand, F. Vitullo, K. Ambrožič, O. Pakari, L. Braun, and D. Godat, "D2.3 Report on the development of fibre-based scintillator," tech. rep., H2020 CORTEX, 2021.
[21] V. Lamirand, M. Hursin, A. Rais, S. Hübner, C. Lange, J. Pohlus, U. Paquee, C. Pohl, O. Pakari, and A. Laureau, "D2.1 Experimental report of the 1st campaign at AKR-2 and CROCUS," tech. rep., H2020 CORTEX, 2018.
[22] V. Lamirand, F. Vitullo, and O. Pakari, "D2.2 Experimental report of the 2nd campaign at AKR-2 and CROCUS," tech. rep., H2020 CORTEX, 2020.
[23] V. Lamirand, A. Knospe, K. Ambrozic, and C. Lange, "D2.4 Experimental report of the 3rd campaign at AKR-2 and CROCUS," tech. rep., H2020 CORTEX, 2021.
[24] W. H. Press, S. A. Teukolsky, W. T. Vetterling, and B. P. Flannery, *Numerical Recipes 3rd Edition: The Art of Scientific Computing*. USA: Cambridge University Press, 3 ed., 2007.
[25] P. Welch, "The use of fast fourier transform for the estimation of power spectra: A method based on time averaging over short, modified periodograms," *IEEE Transactions on Audio and Electroacoustics*, vol. 15, no. 2, pp. 70–73, 1967.
[26] P. Vinai, K. Ambrozic, A. Brighenti, C. Demaziére, B. Gasse, D. Ginestar, M. Hursin, S. Hübner, A. Knospe, V. Lamirand, C. Lange, A. Laureau, R. Macian, A. Mylonakis, O. Pakari, A. Rais, A. Rauchon, S. Santandrea, Z. Stankovski, G. Verdú, A. Vidal-Ferràndiz, T. Yamamoto, H. Yi, S. Yum, I. Zmirajevic, and A. Zoia, "D2.5 Final validation report," tech. rep., H2020 CORTEX, 2021.
[27] K. Ambrožič, V. Lamirand, A. Knospe, F. Vitullo, S. Hübner, O. Pakari, M. Hursin, A. Rais, C. Lange, A. Laureau, P. Frajtag, C. Fiorina, and A. Pautz, "Postprocessing of experimental time series to determine reliable mean and uncertainties." Submitted to Annals of Nuclear Energy, special CORTEX project issue.
[28] C. Lalanne, "Specification development: Mechanical vibration and shock analysis, volume 5," 2014.
[29] N. Letzepis, "On the von mises approximation for the distribution of the phase angle between two independent complex gaussian vectors," in *2015 IEEE International Conference on Acoustics, Speech and Signal Processing (ICASSP)*, pp. 3247–3251, 2015.
[30] W. Härdle, J. Horowitz, and J.-P. Kreiss, "Bootstrap methods for time series," *International Statistical Review*, vol. 71, no. 2, pp. 435–459, 2003.
[31] A. Zoubir, "Bootstrap based spectral analysis," in *IEEE/SP 13th Workshop on Statistical Signal Processing, 2005*, pp. 1310–1315, 2005.
[32] G. Van Rossum and F. L. Drake Jr, *Python reference manual*. Centrum voor Wiskunde en Informatica Amsterdam, 1995.
[33] G. Van Rossum and F. L. Drake, *Python 3 Reference Manual*. Scotts Valley, CA: CreateSpace, 2009.
[34] P. Virtanen, R. Gommers, T. E. Oliphant, M. Haberland, T. Reddy, D. Cournapeau, E. Burovski, P. Peterson, W. Weckesser, J. Bright, S. J. van der Walt, M. Brett, J. Wilson, K. J. Millman, N. Mayorov, A. R. J. Nelson, E. Jones, R. Kern, E. Larson, C. J. Carey, İ. Polat, Y. Feng, E. W. Moore, J. VanderPlas, D. Laxalde, J. Perktold, R. Cimrman, I. Henriksen, E. A. Quintero, C. R. Harris, A. M. Archibald, A. H. Ribeiro, F. Pedregosa, P. van Mulbregt, and SciPy 1.0 Contributors, "SciPy 1.0: Fundamental Algorithms for Scientific Computing in Python," *Nature Methods*, vol. 17, pp. 261–272, 2020.
[35] C. R. Harris, K. J. Millman, S. J. van der Walt, R. Gommers, P. Virtanen, D. Cournapeau, E. Wieser, J. Taylor, S. Berg, N. J. Smith, R. Kern, M. Picus, S. Hoyer, M. H. van Kerkwijk, M. Brett, A. Haldane, J. Fernández del Río, M. Wiebe, P. Peterson, P. Gérard-Marchant, K. Sheppard, T. Reddy, W. Weckesser, H. Abbasi, C. Gohlke, and T. E. Oliphant, "Array programming with NumPy," *Nature*, vol. 585, p. 357–362, 2020.
[36] R. Okuta, Y. Unno, D. Nishino, S. Hido, and C. Loomis, "Cupy: A numpy-compatible library for nvidia gpu calculations," in *Proceedings of Workshop on Machine Learning Systems (LearningSys) in The Thirty-first Annual Conference on Neural Information Processing Systems (NIPS)*, 2017.
[37] J. M. Ortega, *Introduction to FORTRAN 90 for Scientific Computing*. USA: Oxford University Press, Inc., 1st ed., 1994.
[38] V. Lamirand, F. Vitullo, and O. Pakari, "D2.2 experimental report of the 2nd campaign at akr-2 and crocus," tech. rep., H2020 CORTEX, 2020.
[39] D. Padua, ed., *Message Passing Interface (MPI)*, pp. 1116–1116. Boston, MA: Springer US, 2011.
[40] L. Dalcin and Y.-L. L. Fang, "mpi4py: Status update after 12 years of development," *Computing in Science Engineering*, vol. 23, no. 4, pp. 47–54, 2021.
[41] S. Cook, *CUDA Programming: A Developer's Guide to Parallel Computing with GPUs*. San Francisco, CA, USA: Morgan Kaufmann Publishers Inc., 1st ed., 2012.